Growth Analysis of Single-walled Carbon Nanotubes Based on Interatomic Potentials by Molecular Dynamics Simulation

Kaoru Hisama,† Ryo Yoshikawa,† Teppei Matsuo,† Takuya Noguchi,† Tomoya Kawasuzuki,† Shohei Chiashi,† and Shigeo Maruyama*,†,‡

†*Department of Mechanical Engineering, the University of Tokyo*
‡*Energy NanoEngineering Laboratory, National Institute of Advanced Industrial Science and Technology (AIST)*

E-mail: maruyama@photon.t.u-tokyo.ac.jp
Phone: +81-3-5841-6421. Fax: +81-3-5800-6983

Abstract

Molecular dynamics (MD) simulation was performed to understand the growth mechanism of single-walled carbon nanotubes (SWNTs) by using the Brenner-Tersoff potential as the interaction among carbon atoms (C-C), and the Tersoff-type potential as the interaction between carbon and metal (C-M) and between metal and metal atoms (M-M). The potential functions for C-M and M-M bonds were established from the results of *ab initio* calculations. The growth of high-quality SWNTs was simulated at a suitable temperature and supply ratio of carbon atoms. The potential energy of carbon atoms was strongly dependent on the number of C-C and C-M bonds. The dependence explains the growth process, including cap formation, its lift-off, and the continuous SWNT growth.

Introduction

Single-walled carbon nanotubes (SWNTs)[1] have tube structures that consist of sp^2 bonds of carbon atoms as rolled-up graphene sheets. SWNTs exhibit some excellent and unique properties, such as high mechanical strength, high thermal conductivity, and high chemical stability. Some properties, such as electric conductivity, the band gap, and optical properties, are strongly dependent on the tube diameter (d_{tube}) or the chirality (n,m) of the SWNTs. It is thus important to control the SWNT structure for applications that utilize the remarkable properties of SWNTs.

As-grown SWNT samples typically contain SWNTs with various chiralities. Therefore, to obtain structure-controlled SWNT samples, separation or purification processes[2,3] are often used after synthesis. These processes make it possible to extract SWNTs with specific chirality, although dispersants or sonication processes are required, which can cause degradation of the SWNT properties or the formation of defect structures. Chirality-selective growth has recently been reported.[4,5] However, the obtainable chirality was limited and the yield was low.

To date, it has been quite difficult to obtain chirality-selected SWNTs during the growth stage. One of the reasons for this difficulty is that the growth mechanism of SWNTs remains unclear. Chemical vapor deposition (CVD) method is often used for SWNT synthesis. At high temperatures ($\sim$ 900 °C), the carbon source gas is supplied to metal nanoparticles (catalyst particles) and SWNTs are then grown from the catalysts. SWNT growth is depen-

dent on the CVD conditions, such as the temperature, carbon source species, pressure, and flow rate. Many parametric studies for various CVD growth methods and *in situ* observations of SWNT growth[6–8] have been performed. Although the growth mechanism has been intensively investigated, it is still under discussion, and especially the detailed behavior of carbon atoms during growth at the atomic scale is unclear.

Theoretical or simulation approaches are effective for the investigation of phenomena on catalysts at the atomic scale. The mechanism for SWNT growth is generally understood as follows. First, molecules of the carbon source, which are thermally decomposed under certain conditions, are adsorbed onto the metal catalyst particles. The molecules are chemically decomposed on the catalyst and supply carbon atoms.[9] Second, the carbon atoms diffuse on the catalysts while they interact with metal atoms.[10–12] The carbon atoms bind with each other and form carbon-carbon hemispherical networks (cap structures) on the catalyst surface.[13,14] Finally, after the cap structure lifts off from the catalyst surface,[15] SWNT growth begins.[16,17]

The growth process involves various chemical reactions among carbon and metal atoms, including molecular decomposition in the gas phase, and these reactions are separately analyzed using density functional theory (DFT) calculations.[9,18] However, DFT calculations are computationally expensive and it is impossible to calculate the entire growth process. Therefore, to clarify the growth mechanism, it is important to comprehensively understand the phenomena that occur on the catalyst at the atomic scale. In this study, new empirical potential functions were developed that describe the interaction between carbon and metal atoms, and molecular dynamics (MD) simulation was performed using the potential functions. The potential functions were obtained on the basis of DFT calculation results. To focus on the reactions and the behavior of carbon and metal atoms, thermal or catalytic decomposition processes of the carbon source molecules were omitted by directly supplying atomic carbon to the metal catalyst particles (Co or Fe).

Simulation method

MD simulations were performed under temperature control with the Nośe-Hoover thermostat. The time step was 0.5 fs. A simulation cell size was $10 \times 10 \times 10\,\mathrm{nm}^3$ and a periodic condition was imposed along the three axis directions. A metal cluster composed of 60 metal atoms (Co or Fe) was used as the SWNT growth catalyst particle. A spherical cluster was obtained after structural relaxation for 2 ns. For the growth simulation, atomic carbon was added into the simulation cell while maintaining the number of carbon atoms in the gas phase, n_{free}, constant. The initial kinetic energy of the atomic carbons was $(3/2)\,k_{\mathrm{B}}T$, where T is the growth temperature, and atomic carbon was supplied in a random direction. Interactions between atoms are expressed by empirical potential functions, which are the simplified Brenner-Tersoff potential[19] for carbon-carbon (C-C) bonds, Tersoff-type potentials for both metal-metal (M-M) and carbon-metal (C-M) bonds, and the Lennard-Jones potential (ϵ = 2.4 meV, σ=3.37 Å) for long-term interactions between C-C.

The Tersoff-type potentials for M-M and C-M bonds were developed following the scheme given in the literature.[20]

Various types of atomic structures of carbon and metal atoms (dimer, regular triangle, chain, diamond, simple cubic (SC), base-centered cubic (BCC), face-centered cubic (FCC), and hexagonal close packed (HCP)) including the configurations of graphene and metal atoms, were considered. Using commercial calculation software (Vienna *Ab initio* Simulation Package, VASP[21,22]) based on DFT, the most stable positions of atoms for each of the structures were calculated, and the lattice constant and cohesive energy were then obtained. The parameters of the Tersoff-type potentials were optimized to reproduce the most stable structure with respect to the cohesive energy using a genetic algorithm method. (See more details on

the development of the empirical potential functions in the Supplementary Information.)

Results and discussion

Figure 1(A) shows snapshots of the MD simulation of SWNT growth from a Co catalyst with a carbon supply rate of n_{free}=3 at 1500 K. The blue balls represent metal atoms and the others are carbon atoms. The white, red, yellow, and green carbon atoms represent those carbon atoms that are chemically bonded with zero, one, two, and three other carbon atom(s), respectively. In advance, 60 Co atoms were annealed at 1500 K for 2 ns and they then formed a spherical cluster with a diameter of 1.0 nm (t = 0.0 ns). Supplied carbon atoms collided with and adsorbed onto the Co catalyst nanoparticle, and carbon and metal atoms became mixed (t = 10.0 ns). After the catalyst contained a sufficient number of carbon atoms, the carbon atoms with two and three carbon-carbon (C-C) bonds (yellow and green spheres in Fig. 1) became prominent on the surface and they gradually formed a cap structure (t = 50.0 ns). The cap lifted off the catalyst (t = 100.0 ns) and then an SWNT started to grow (t = 200.0 ns). While the wall edge of the SWNT was stably connected to the catalyst, the wall part of the SWNT grew continuously (t = 300.0 and 600.0 ns). Carbon atoms diffusing on the catalyst reached the connection edge, and some of these were incorporated into the SWNT wall.

Each step of SWNT growth that was observed in MD simulation, such as carbon atom diffusion,[10,11] cap formation,[15] cap lift-off[15,23] and SWNT wall extension,[16,17] has already been reported in MD calculation researches. However, in this study, we succeeded in simulating the entire process of SWNT growth and obtained a high-quality SWNT, as shown in Fig. 1(A). In Fig. 2, the developed view of the SWNT wall part (Fig. 1(A)) is shown. Although five- and seven-membered rings were formed, they appeared as adjacent pairs in many cases. Therefore, the SWNT straightly grew up. Figure 2(B, C) show the time variation of the numbers of five-, six-, and seven-membered carbon rings of the SWNT during growth from the Co and Fe catalysts, respectively. The increase in the total number of carbon rings indicated SWNT growth, which was almost proportional to the growth time. The ratio of five- and seven-membered rings after lift-off was almost constant during the growth simulation, which indicates that such a defective atomic structure was stochastically formed. The ratio of six-membered rings in the cases of Co and Fe catalysts was approximately 76 and 56%, respectively. To the best of our knowledge, the grown SWNT, as shown in Fig. 1(A), is the longest SWNT (4 nm in length) with the highest quality obtained by simple MD simulation. Note that the growth process, including the cap-formation, lift-off, and the growth of the wall parts, are reproducible under the growth conditions.

When the growth temperature was relatively low (T < 1300 °C) or the carbon supply rate was relatively high (typically $n_{\mathrm{free}} \geq 6$), the SWNT did not grow. Under these conditions, multiple cap structures were formed on the catalyst surface, and these caps converged into one large cap that covered the entire surface of the catalyst, as shown in Fig. 1(C). If the catalyst was covered with too large a cap, then lift-off could not occur and the catalyst was finally encapsulated by the carbon shell.

To understand the growth process of SWNTs more easily, the carbon atoms were categorized into three groups with respect to the bond configuration. The first group is a carbon atom that has more than four bonds with metal atoms (C-M bond) as an "inner carbon", which was located inside the catalyst. The second group is a carbon atom that has one to four C-M bond(s) as "surface carbon", and the third group is a carbon atom without a C-M bond as "cap carbon" or "tube carbon". Figure 3(A, B) show the number of SWNT carbon atoms (and/or cap carbon atoms), the surface and inner carbon atoms during growth. The inner carbon atoms immediately increased after carbon supply. In the case of Co catalyst, around 50 ns, the number of cap carbon atoms rapidly increased, although the number of inner carbon atoms slightly decreased.[24] This cor-

responded to a cap lift-off. After lift-off, the number of inner carbons was constant and that of the tube carbons gradually increased, which corresponded to SWNT growth. During stable growth (after 150 ns), the carbon adsorption rate was in equilibrium with the growth rate, which suggests that the growth under these conditions was pressure-limited. The number of inner carbon for Co catalyst was almost the same as that for Fe catalyst, which was approximately 10 atoms. The cabon solubility was 15% and the Lindemann index calculation[25] revealed that the Co and Fe catalysts dissolving 10 carbon atoms was in the liquid phases.

The enlarged image around the interface of the SWNT and the catalyst shown in Fig. 3(C, D) exhibits a clear border between the two domains of surface (purple) and tube carbons (green). The border part is regarded as the growth region of the SWNT. The surface carbon atoms frequently change bonds with carbon and metal atoms, which could be regarded as a catalyst effect, while the cap and tube carbons did not change at all in this temperature range. Therefore, the cap and wall parts of the SWNT were fixed after detachment from the catalyst.

The number of surface carbons in the growth region on the Co catalyst (approximately 80 carbon atoms in Fig. 3(C)) was larger than that on an Fe catalyst (approximately 20 carbon atoms in Fig. 3(D)), and especially, some linear chains of carbon atoms [26,27] appeared on the Co catalyst. On the other hand, the growth rate with the Fe catalyst was much higher than that with the Co catalyst. The growth difference between Co and Fe catalyst comes from the surface diffusion of carbon atoms on the catalyst. The residence time is defined by the time period from the adsorption on the catalyst to the detachment from the catalyst. The average residence time was 92 ns for Co and 22 ns for Fe catalyst, respectively. In the case of Co catalyst, most of the carbon atoms on the catalyst surface formed the chain structure. The chain structure decreased the surface diffusion of carbon atoms.

Next, we discuss the difference in SWNT growth between Co and Fe catalysts based on the interaction potentials between carbon and metal atoms. In order to simplify the discussion, the dissociation energy of carbon atom i, $E_i^{\rm dis}$, is defined as

$$E_i^{\rm dis} = \frac{1}{2}\sum_{i\neq j}\phi_{ij}, \qquad (1)$$

where ϕ_{ij} is the potential energy between atoms i and j (see details in the Supporting Information). Figure 4 shows $E_i^{\rm dis}$ of carbon atoms with different numbers of C-C and C-M bonds during the growth process for (A) Co and (B) Fe catalysts. During the early stage of free carbon supply, the density of carbon atoms on the catalyst was low and the carbon atoms could form only one C-C bond at most. With an increase in the number of C-M bonds, $E^{\rm dis}$ decreased for carbon atoms without C-C bonds or with only one C-C bond, as shown in Fig. 4. Therefore, most of the carbon atoms were located within the catalyst and formed more than four C-M bonds.

When the carbon density became sufficiently high, carbon atoms started to form multiple C-C bonds. $E^{\rm dis}$ for the carbon atoms with two or three C-C bonds decreased with the number of C-M bonds; therefore, carbon atoms that appeared on the catalyst surface increased C-C bonds and decreased C-M bonds. On the metal surface, $E^{\rm dis}$ for a carbon atom with one C-M bond and three C-C bonds was the lowest, which induced the formation of the sp^2 bonding structure. The sp^2 network gradually grew to be the cap-structure of the SWNT, as shown in Fig. 1(A). The mechanism for formation of the cap-structure was common for both the Co and Fe catalysts.

While $E^{\rm dis}$ with C-M bond is lower than that without C-M bond for carbon atoms with zero-two C-C bond(s), $E^{\rm dis}$ without C-M bond is lower than that with C-M bond(s) for carbon atoms with three C-C bonds. This means that only carbon atoms with three C-C bonds possibly detach from the catalyst surface by breaking C-M bonds. The detachment induced the lift-off of the cap-structure and growth of the SWNT. Note that temporary detachment was observed for carbon atoms with two C-C bonds, and carbon atoms without a C-C bond or only

one C-C bond were never detached in the simulation.

Although E^{dis} for the carbon atom decreased due to detachment from the catalyst surface, the detachment increased the total energy of the other carbon atoms and the metal atoms, as shown in Fig. 4. However, if the carbon atoms diffusing on the catalyst surface continuously reached the growth region, then detachment could successively occur, which would mean that SWNT growth would continue. This indicates that the E^{dis} difference of the carbon atoms that have three C-C bonds between with and without a C-M bond is one of the driving forces of SWNT growth. This energy difference with the Fe catalyst was larger than that with the Co catalyst, and the large energy difference promoted detachment and the SWNT growth rate. Eventually, the growth rate for the Fe catalyst (3.0×10^{-2} m/s) was higher than that for the Co catalyst (0.6×10^{-2} m/s) with $n_{\mathrm{free}} = 3$. On the other hand, the side-wall part with the Fe catalyst contained more defect structures than that with the Co catalyst. The higher growth rate reduced the possibility of six-membered ring formation and induced the formation of defect structures (five- or seven-membered rings).

Finally, the temperature dependence of SWNT growth is discussed. Figure 5 shows the temperature dependence of the surface carbon numbers with different numbers of C-C bonds during the growth simulation. The surface carbon atoms with two or three C-C bonds were the majority, and the generation and decomposition rates of C-C bonds were thermally balanced. At lower temperatures (~ 1300 K), the entire surface area was often covered with carbon atoms, and the catalyst was deactivated because the number of carbon atoms with three C-C bonds was too large. As the temperature increased, the total numbers of carbon atoms and carbon atoms with three C-C bonds decreased on the catalyst surface. The carbon atoms with two C-C bonds diffused more actively at higher temperature and this feature improved the crystal structure quality of the resultant SWNTs.

Conclusion

MD simulation was performed to analyze the SWNT growth process. Under appropriate conditions of temperature and carbon supply rate n_{free}, SWNT growth with high quality was simulated. The change of the potential energy of carbon atoms during growth simulation was investigated and it was confirmed that the potential energy differs depending on the numbers of C-C and C-M bonds that each carbon atom has. This suggests that the potential energy change of carbon atoms depends on the numbers of bonds and has an important role in SWNT growth.

figures

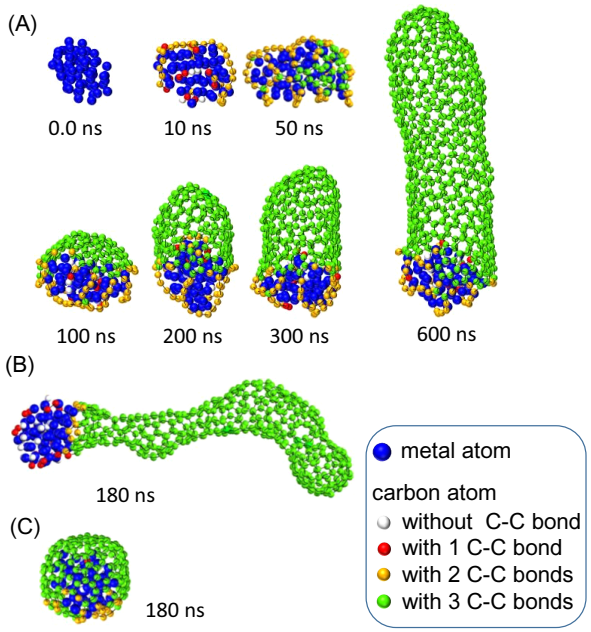

Figure 1: Snapshots of the SWNT growth process from (A) Co and (B) Fe catalysts. The blue balls represent metal atoms, while the white, red, orange, and green balls represent carbon atoms with different numbers of C-C bonds. The growth temperature was 1500 K with $n_{\mathrm{free}} = 3$. (C) Deactivated Co catalyst due to encapsulation by a carbon shell.

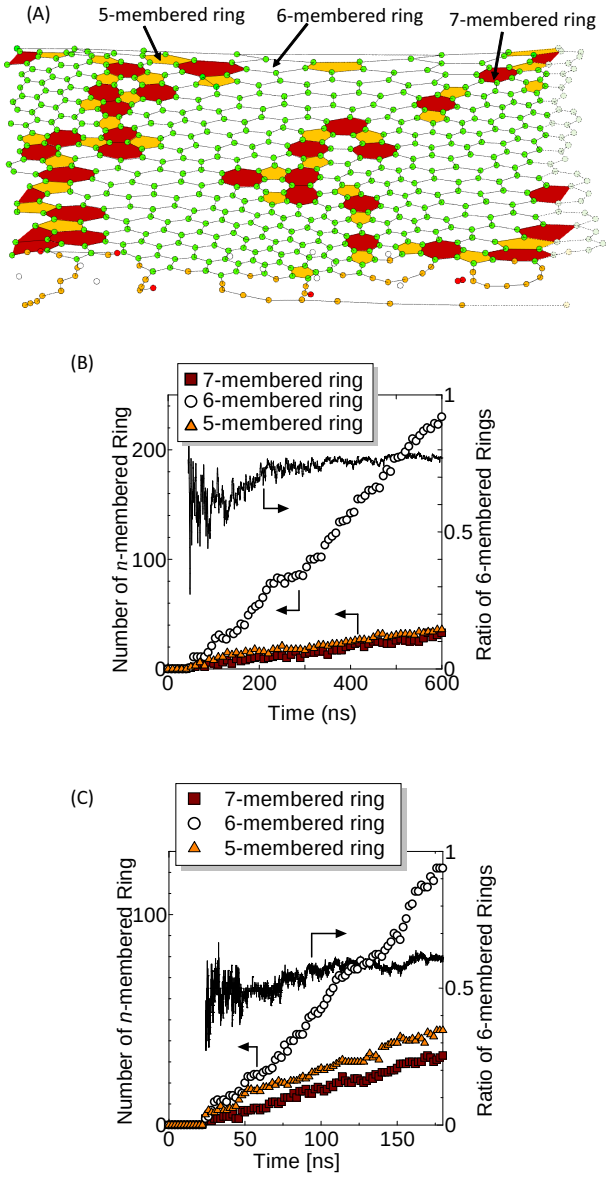

Figure 2: (A) Developed view of the SWNT grown from Co catalyst, as shown in Fig. 1(A). Numbers of the total, five-, six-, and seven-membered carbon rings and the ratio of 6-membered rings during SWNT growth from (B) Co and (C) Fe catalysts.

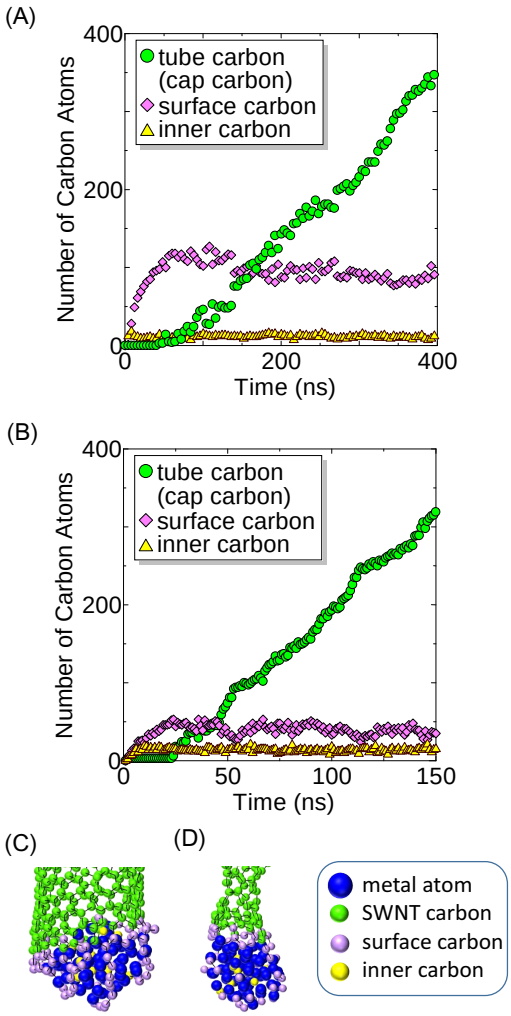

Figure 3: Number of carbon atoms during SWNT growth from (A) Co and (B) Fe catalysts. Snapshot of the structure around the growth region of the (C) Co and (D) Fe catalysts. The yellow, purple, and green carbon atoms represent the inner, surface, and cap/tube carbon atoms, respectively.

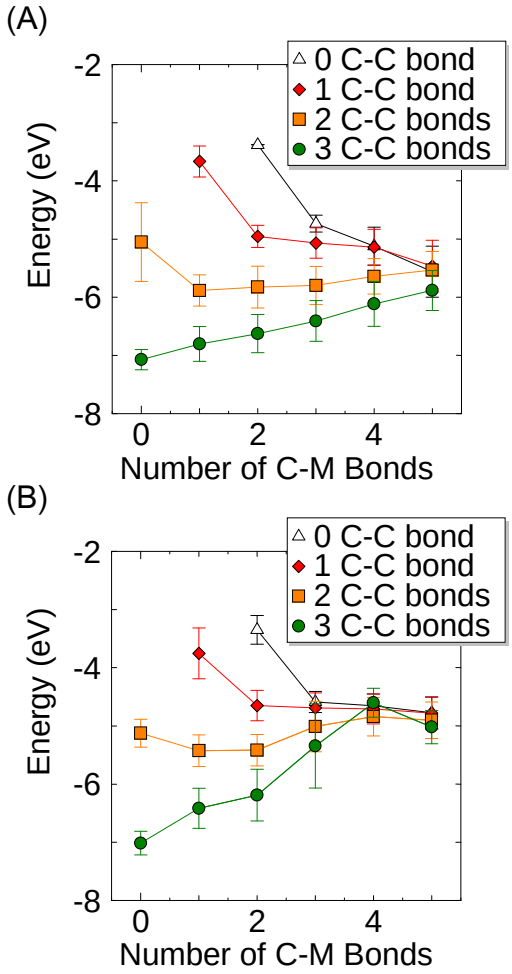

Figure 4: Dissociation energy (E^{dis}) of carbon atoms with different number of the chemical bonds (C-C and C-M bonds) during the SWNT growth from the (A) Co and (B) Fe catalysts.

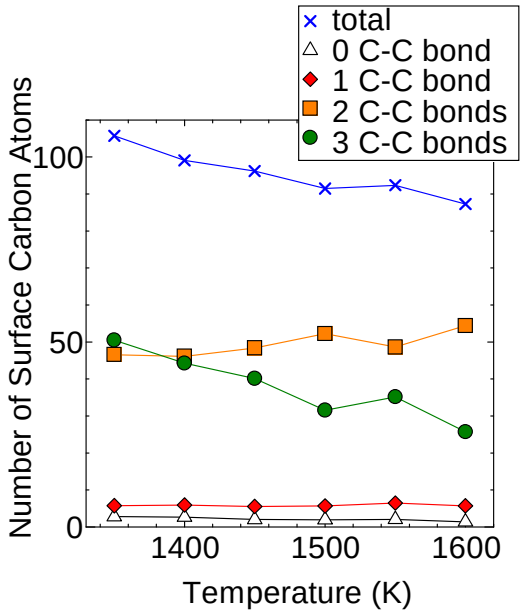

Figure 5: Temperature dependence of the number of carbon atoms with different numbers of C-C bonds on the Co catalyst surface.

Supporting Information

The Supporting Information is available free of charge on theACS Publications website.

The details of the potential function among carbon atoms, and the development of Tersoff-type potential for metal atoms and for compounds with carbon and metal atoms.

Acknowledgement

The part of this work was financially supported by JSPS KAKENHI Grant Numbers JP15H05760, JP25107002, and JP17K06187. and the IRENA Project of JST-EC DG RTD, Strategic International Collaborative Research Program (SICORP).

References

(1) Iijima, S.; Ichihashi, T. Single-Shell Carbon Nanotubes of 1-nm Diameter. *Nature* **1993**, *363*, 603–605.

(2) Arnold, M. S.; Green, A. A.; Hulvat, J. F.; Stupp, S. I.; Hersam, M. C. Sorting Carbon Nanotubes by Electronic Structure

Using Density Differentiation. *Nat. Nanotechnol.* **2006**, *1*, 60–65.

(3) Tu, X.; Manohar, S.; Jagota, A.; Zheng, M. DNA Sequence Motifs for Structure-Specific Recognition and Separation of Carbon Nanotubes. *Nature* **2009**, *460*, 250–253.

(4) Yang, F.; Wang, X.; Zhang, D.; Yang, J.; Luo, D.; Xu, Z.; Wei, J.; Wang, J.; Xu, Z.; Peng, F. et al. Chirality-specific Growth of Single-Walled Carbon Nanotubes on Solid Alloy Catalysts. *Nature* **2014**, *510*, 522–524.

(5) Sanchez-Valencia, J. R.; Dienel, T.; Gröning, O.; Shorubalko, I.; Mueller, A.; Jansen, M.; Amsharov, K.; Ruffieux, P.; Fasel, R. Controlled Synthesis of Single-Chirality Carbon Nanotubes. *Nature* **2014**, *512*, 61–64.

(6) Sharma, R.; Iqbal, Z. *In Situ* Observations of Carbon Nanotube Formation Using Environmental Transmission Electron Microscopy. *Appl. Phys. Lett.* **2004**, *84*, 990–992.

(7) Yoshida, H.; Takeda, S.; Uchiyama, T.; Kohno, H.; Homma, Y. Atomic-Scale In-Situ Observation of Carbon Nanotube Growth from Solid State Iron Carbide Nanoparticles. *Nano Lett.* **2008**, *8*, 2082–2086.

(8) Einarsson, E.; Murakami, Y.; Kadowaki, M.; Maruyama, S. Growth Dynamics of Vertically Aligned Single-Walled Carbon Nanotubes from In Situ Measurements. *Carbon 46:923-930* **2008**, *46*, 923–930.

(9) Oguri, T.; Shimamura, K.; Shibuta, Y.; Shimojo, F.; Yamaguchi, S. Ab Initio Molecular Dynamics Simulation of the Dissociation of Ethanol on a Nickel Cluster: Understanding the Initial Stage of Metal-Catalyzed Growth of Carbon Nanotubes. *J. Phys. Chem. C* **2013**, *117*, 9983–9990.

(10) Yazyev, O. V.; Pasquarello, A. Effectfect of Metal Elements in Catalytic Growth of Carbon Nanotubes. *Phys. Rev. Lett.* **2008**, *100*, 156102–1–156102–4.

(11) Wirth, C. T.; Zhang, C.; Zhong, G.; Hofmann, S.; Robertson, J. Diffusion- and Reaction-Limited Growth of Carbon Nanotube Forests. *ACS Nano* **2009**, *3*, 3560–3566.

(12) Ribas, M. A.; Ding, F.; Balbuena, P. B.; Yakobson, B. I. Nanotube Nucleation versus Carbon-Catalyst Adhesion-Probed by Molecular Dynamics Simulations. *J. Chem. Phys.* **2009**, *131*, 224501–1–224501–7.

(13) Ohta, Y.; Okamoto, Y.; Page, A. J.; Irle, S.; Morokuma, K. Quantum Chemical Molecular Dynamics Simulation of Single-Walled Carbon Nanotube Cap Nucleation on an Iron Particle. *ACS Nano* **2009**, *3*, 3413–3420.

(14) Neyts, E. C.; Shibuta, Y.; van Duin, A. C. T.; Bogaerts, A. Catalyzed Growth of Carbon Nanotube with Definable Chirality by Hybrid Molecular Dynamics-Force Biased Monte Carlo Simulations. *ACS Nano* **2010**, *4*, 6665–6672.

(15) Shibuta, Y.; Maruyama, S. Molecular Dynamics Simulation of Formation Process of Single-Walled Carbon Nanotubes by CCVD Method. *Chem. Phys. Lett.* **2003**, *382*, 381–386.

(16) Ding, F.; Larsson, P.; Larsson, J. A.; Ahuja, R.; Duan, H. M.; Rosén, A.; Bolton, K. The importance of Strong Carbon-Metal Adhesion for Catalytic Nucleation of Single-Walled Carbon Nanotubes. *Nano Lett.* **2008**, *8*, 463–468.

(17) Neyts, E. C.; van Duin, A. C. T.; Bogaerts, A. Changing Chirality during Single-Walled Carbon Nanotube Growth: A Reactive Molecular Dynamics/Monte Carlo Study. *J. Am. Chem. Soc.* **2011**, *133*, 17225–17231.

(18) Amara, H.; Bichara, C.; Ducastelle, F. Understanding the Nucleation Mechanisms of Carbon Nanotubes in Catalytic Chemical Vapor Deposition. *Phys. Rev. Lett.* **2008**, *100*, 056105–1–056105–4.

(19) Yamaguchi, Y.; Maruyama, S. A Molecular Dynamics Study on the Formation of Metallofullerene. *Eur. Phys. J. D* **1999**, *9*, 385–388.

(20) Kumagai, T.; Hara, S.; Izumi, S.; Sakai, S. Development of a Bond-Order Type Interatomic Potential for Si-B Systems. *Modell. Simul. Mater. Sci. Eng.* **2006**, *14*, S29–S37.

(21) Kresse, G.; Hafner, J. *Ab initio* Molecular Dynamics for Liquid Metals. *Phys. Rev. B* **1993**, *47*, 558–561.

(22) Kresse, G.; Furthmüller, J. Efficient Iterative Schemes for *ab initio* Total-Energy Calculations Using a Plane-Wave Basis Set. *Phys. Rev. B* **1996**, *54*, 11169–11186.

(23) Schebarchov, D.; Hendy, S. C.; Ertekin, E.; Grossman, J. C. Interplay of Wetting and Elasticity in the Nucleation of Carbon Nanotubes. *Phys. Rev. Lett.* **2011**, *107*, 185503–1–185503–5.

(24) Ding, F.; Rosén, A.; Bolton, K. Molecular Dynamics Study of the Catalyst Particle Size Dependence on Carbon Nanotube Growth. *J. Chem. Phys.* **2004**, *121*, 2775–2779.

(25) Nayak, S. K.; Khanna, S. N.; Rao, B. K.; Jena, P. Thermodynamics of Small Nickel Clusters. *J. Phys.: Condens. Matter* **1998**, *10*, 10853–10862.

(26) Raty, J. Y.; Gygi, F.; Galli, G. Growth of Carbon Nanotubes on Metal Nanoparticles: A Microscopic Mechanism from *ab initio* Molecular Dynamics Simulations. *Phys. Rev. Lett.* **2005**, *95*, 096103–1–096103–4.

(27) Diarra, M.; Zappelli, A.; Amara, H.; Ducastelle, F.; Bichara, C. Importance of Carbon Solubility and Wetting Properties of Nickel Nanoparticles for Single Wall Nanotube Growth. *Phys. Rev. Lett.* **2012**, *109*, 185501–1–185501–5.

Graphical TOC Entry